Anomalous Conformational Instability and Hydrogel Formation of a Cationic Class of Self-Assembling Oligopeptides

ARTICLE *in* MACROMOLECULES · AUGUST 2010

Impact Factor: 5.8 · DOI: 10.1021/ma101450b

4 AUTHORS, INCLUDING:

Reinhard Schweitzer-Stenner
Drexel University
219 PUBLICATIONS **4,369** CITATIONS

DOI: 10.1021/ma101450b

Macromolecules
ARTICLE

Anomalous Conformational Instability and Hydrogel Formation of a Cationic Class of Self-Assembling Oligopeptides

Thomas J. Measey,[†] Reinhard Schweitzer-Stenner,*[,†] Vijoya Sa,[‡] and Konstantin Kornev[‡]

[†]*Department of Chemistry, Drexel University, Philadelphia, Pennsylvania 19104, and*
[‡]*School of Materials Science and Engineering, Clemson University, Clemson, South Carolina 29634*

Received June 30, 2010; Revised Manuscript Received August 9, 2010

ABSTRACT: A detailed understanding of the mechanistic principles which govern peptide and protein self-assembly is of considerable biomedical and biotechnological importance. Owing to the diversity of peptide and protein sequences which have been shown to aggregate into ordered structures, the ability to self-assemble is now recognized as an inherent feature of the polypeptide backbone. It is therefore of utmost importance to elucidate the rules governing the self-assembly process. *De novo* designed oligopeptides, based on sequences of alternating hydrophilic and hydrophobic residues and containing complementary charge distributions, have shown the potential to self-assemble into hydrogels rich in β-sheet secondary structure. Here we present and characterize the unexpected self-assembly and hydrogel formation of AK-16, an alanine-rich oligopeptide, whose sequence does not abide by typical rules which allow for peptide self-organization. AK-16 spontaneously forms soluble, thermodynamically unstable β-sheet-rich aggregates, which can be stabilized by salt addition to yield a self-supporting macroscopic hydrogel. The AK-16 hydrogel exhibits the ability to encapsulate and slowly release a model protein. This one-charge-type system represents a novel class of self-assembling oligopeptides, in which the initial conformational instability can be exploited to tune the viscosity and physicochemical properties of the resultant hydrogel. This study provides insight for the future *de novo* design of self-assembling oligopeptides.

Introduction

Molecular self-assembly is governed by noncovalent interactions and is ubiquitous throughout nature and emerging technologies.[1,2] In particular, the spontaneous organization of peptides and proteins is of significant biomedical and biotechnological relevance. The onset of various seemingly unrelated diseases such as Alzheimer's, Huntington's, Parkinson's, and type II diabetes is directly associated with the spontaneous aggregation of specific proteins into filamentous structures, termed amyloid fibrils.[3−5] Despite the sequence diversity of the disease-related proteins, the resulting fibril architectures are remarkably similar, consisting of a "cross-β" core, with individual β-strands aligned perpendicular to the fibril axis.[6,7] The formation of these fibrils has recently been shown to be causative in at least one type of amyloidosis, suggesting that inhibition or prevention of fibril growth offers a therapeutic means to combat many amyloidoses.[8] In this regard, elucidation of the mechanistic principles and contributing interactions which govern the fibril formation process is of utmost importance.

In addition to the biomedical relevance, peptide self-assembly has been exploited in recent years to create materials with inherent biofunctionality and biocompatibility. In particular, peptide hydrogels have shown potential to act as drug delivery systems[9,10] and tissue engineering scaffolds[11,12] and to accelerate hemostasis.[13] *De novo*-designed oligopeptide systems typically rely on a sequence of alternating hydrophobic and hydrophilic residues, often containing complementary charge distributions recurring throughout.[2] Examples of such systems include KLD-12 (AcN-$(KLDL)_4$-CNH_2),[14] RADA-16 (AcN-$(RARADADA)_2$-CNH_2),[9,10] EAK-16 ($(AEAEAKAKA)_2$),[12] EMK16-II ($(MEMEMKMK)_2$),[15] and MAX-1 ($(VK)_4V^DPPT(KV)_4$-NH_2).[16] Each of these peptides can form a polymeric network of nanofibers under well-defined conditions, e.g., pH, temperature, etc., rich in β-sheet secondary structures.

In particular, the oligopeptides KLD-12, RADA-16, EAK-16, and EMK-16 all possess charged side chains under neutral pH conditions, which are positioned in the sequence so as to allow for favorable electrostatic interactions which stabilize β-sheet secondary structures. Recently, however, a comparison of the self-aggreagation of EMK16-II and EAK-16 led to the conclusion that hydrophobic rather than electrostatic interactions are the driving force of aggregation.[15] To advance the exploitation of peptide self-assembly for the creation of novel biomaterials, it is necessary to have a complete and detailed understanding of the rules which govern the self-assembly process.

In contrast to *de novo* designed oligopeptide sequences containing alternating complementary charges, our group has recently reported the surprising ability of an alanine-based peptide, namely Ac-$(AAKA)_4$-NH_2 (AK-16), to form a hydrogel rich in β-sheet structures.[17] Here, we present the anomalous conformational instability of soluble AK-16 β-sheet aggregates. Stabilization of the initial AK-16 β-sheet structures via salt addition yields a macroscopic hydrogel which can slowly release encapsulated molecules. The viscosity and physicochemical properties of the AK-16 hydrogels can by tuned by varying the type of salt as well as the salt and peptide concentrations and more importantly by exploiting the conformational instability of the β-sheet aggregates. These unique properties are, in part, promoted by the length of the lysine side chains. Our results illustrate the unique properties of a novel class of self-assembling peptides and provide insight into considerations for *de novo* design of self-assembling oligopeptides.

Results

Time-Dependent UV-CD Spectra Reflects Conformational Instability of AK-16. Upon dissolution in deuterated water,

*Corresponding author: Tel (215)-895-2268; Fax (215)-895-1265; e-mail Rschweitzer-stenner@drexel.edu.

 Published on Web 08/18/2010

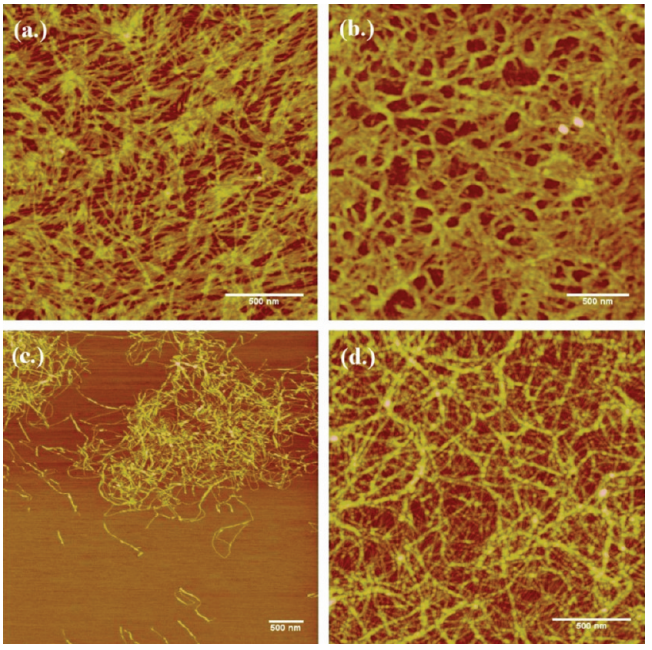

Figure 1. AFM height images of various samples deposited onto freshly cleaved mica. (a) 10 mg/mL AK-16 solution, showing a filamentous network. (b) AK-16 hydrogel, prepared with AK-16 and NaCl concentrations of 10 mg/mL and 1.0 M, respectively, displaying a nanoweb-like network. (c) 50 μg/mL (35 μM) AK-16, showing bundles of filaments. (d) 5 mg/mL AR-16 solution, showing structures similar to those of AK-16. The scale bar in each image represents 500 nm.

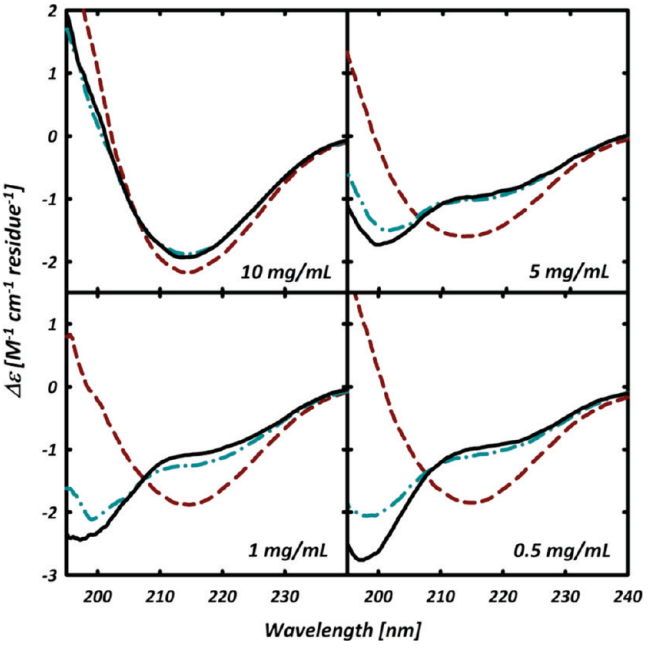

Figure 2. Time-dependent UV-CD spectra of AK-16 at various concentrations. For clarity, only those spectra acquired at 300 s (short dash), 9000 s (dash-dot-dash), and 18 000 s (solid) minutes after dissolution in deuterated water are shown. The spectral changes reflect a decrease in β-sheet secondary structure, while the increase in the negative maximum at 198 nm reflects an increase in more flexible PPII- and turn-like conformations as described in the text.

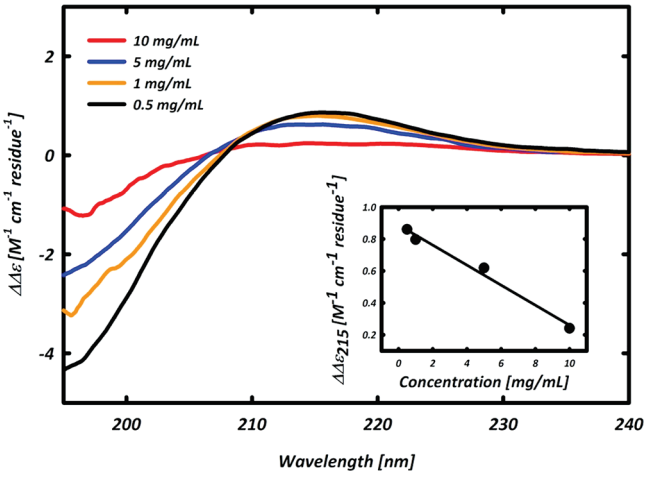

Figure 3. UV-CD difference spectra of the time-dependent AK-16 UV-CD spectra shown in Figure 2 (18 000−300 s). Inset: extinction coefficient at 215 nm of the difference spectra as a function of AK-16 concentration.

AK-16 immediately forms a thermodynamically unstable population of β-sheet-rich structures. This is observed even at concentrations as low as 7 μM. These β-sheet rich aggregates organize into a filamentous network of structures, as shown in Figure 1a, and exhibit the ability to bind the amyloid-specific dye Congo Red (Figure S1), consistent with other oligopeptide aggregates[15] and indicative of structures very similar to those of amyloid fibrils.[18] At lower concentrations, bundles of fibril-like structures are observed, as shown in Figure 1c for a 35 μM solution of AK-16. In contrast to amyloid-like fibrils, however, the AK-16 aggregates are soluble and conformationally unstable. Figure 2 exhibits representative time-dependent UV-circular dichroism (UV-CD) spectra of AK-16 at various peptide concentrations. For each concentration, the spectrum measured after 5 min of sample preparation exhibit a negative maximum at ca. 215 nm, indicative of a β-sheet conformation.[19] As time progresses, this band slowly loses intensity at the expense of a negative maximum appearing at ~198 nm and a negative shoulder near 220 nm, for concentrations ≤5 mg/mL (3.5 mM). These spectral changes reflect a conformational transition into more poly-L-proline II (PPII)- and possible turn-like conformations.[20] The difference spectra between those measured at 18 000 s (300 min) and 300 s (5 min) exhibit a characteristic positive maximum at 218 nm and a negative maximum at 198 nm (see Figure 3), both of which are consistent with a predominance of PPII-like conformations being populated.[21]

The kinetics of the above conformational transitions probed by recording the dichroism at 215 nm, $\Delta\varepsilon_{215}$, as a function of time for three different peptide concentrations exhibit clear biphasic behavior (Figure 4). The fast phase is concentration-independent and has a time constant of 18 ± 1 min, while the second phase proceeds an order of magnitude slower and yields a time constant which is linearly proportional to the peptide concentration, as depicted in the inset of Figure 4. As will be discussed, the fast phase reflects the slow hydration of the AK-16 aggregates. It should be noted that the kinetic data shown in Figure 4 cannot be directly compared with the representative spectra shown in Figure 2, since fresh solutions were used for the kinetic experiments as described in the Materials and Methods section.

Time-Dependent FTIR Confirms Slow Hydration Kinetics of AK-16. To further elucidate structural characteristics of the unstable AK-16 aggregates, we measured the time-dependent Fourier transform infrared (FTIR) spectra of AK-16 in the amide I′ band region. The amide I′ band is the most structurally sensitive IR band, resulting predominantly from backbone carbonyl stretching.[22] The FTIR spectra of the amide I′ band region of AK-16 (10 mg/mL), measured at 300 s (5 min) and 18 000 s (300 min) after

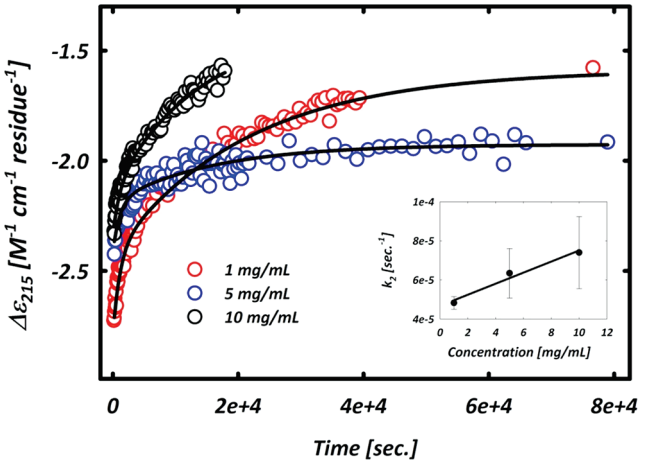

Figure 4. Kinetic analysis of AK-16 at three different peptide concentrations, namely 1, 5, and 10 mg/mL, probed at 215 nm. The decay of the 215 nm signal reflects the loss of β-sheet structure. An analysis revealed biphasic kinetics, consisting of a concentration-independent fast phase with a time constant of 18 ± 1 min attributed to the slow hydration kinetics of AK-16 β-sheet aggregates. The second phase proceeds an order of magnitude slower that the first, with the rate constant, k_2, exhibiting a linear correlation with the concentration of AK-16, as shown in the inset.

dissolution, are shown in Figure 5. An intense band at 1618 cm^{-1} and a much weaker band at 1693 cm^{-1} are consistent with an antiparallel β-sheet conformation.[23] Further support for such an antiparallel arrangement has recently been provided by molecular dynamics (MD) simulations of AK-16 dimers and trimers.[24]

Interestingly, the FTIR spectrum of AK-16 initially shows some intensity in the amide II band region (Figure 5a). This band typically occurs between 1500 and 1600 cm^{-1} and results from a combination of C−N (s), C−C (s) (s = stretching mode), and N−H in-plane bending.[22] Deuteration results in a downshift of the amide II band (termed amide II′) by ~100 cm^{-1}, owing to the lower frequency of the N−D bending.[25] This initial intensity in the amide II region of the initial AK-16 spectrum indicates a significant amount of amide protons involved in hydrogen bonds. These amide protons slowly exchange with deuterons of the solvent, resulting in a decrease in intensity of the amide II band and a concomitant increase in intensity of the amide II′ band. A linear correlation exists between the amide II′ and amide II peak intensities, suggesting a slow H−D exchange process. Interestingly, the kinetics probed by both the amide II′ and amide II peak intensities can be fit with a single-exponential function with the time constant determined for the fast phase of the UV-CD kinetic analysis, namely 18 ± 1 min. This value is indicative of somewhat buried, immobile amide protons.[26]

Side Chain Length Promotes Conformational Instability. In an attempt to elucidate the stabilizing elements of AK-16 β-sheet aggregates, we explored to what extent the substitution of lysine by other charged residues would affect the peptides propensity for self-aggregation. In particular, the four lysine residues in AK-16 were substituted by either glutamic acid (E), arginine (R), or ornithine (O), resulting in the following sequences: Ac-$(AAEA)_4$-NH_2 (AE-16), Ac-$(AARA)_4$-NH_2 (AR-16), and Ac-$(AAOA)_4$-NH_4 (AO-16), respectively. Ornithine is essentially a truncated lysine residue, with one fewer methylene ($-CH_2$) group. In addition, we also investigated Ac-$(AAKA)_3$-NH_2 (AK-12) to see if sequence length played a role in the aggregation propensity of AK-16. Figure 6 shows the UV-CD spectra of AO-16, AE-16, and AK-12 in deuterated water at different pH values, all of which are at

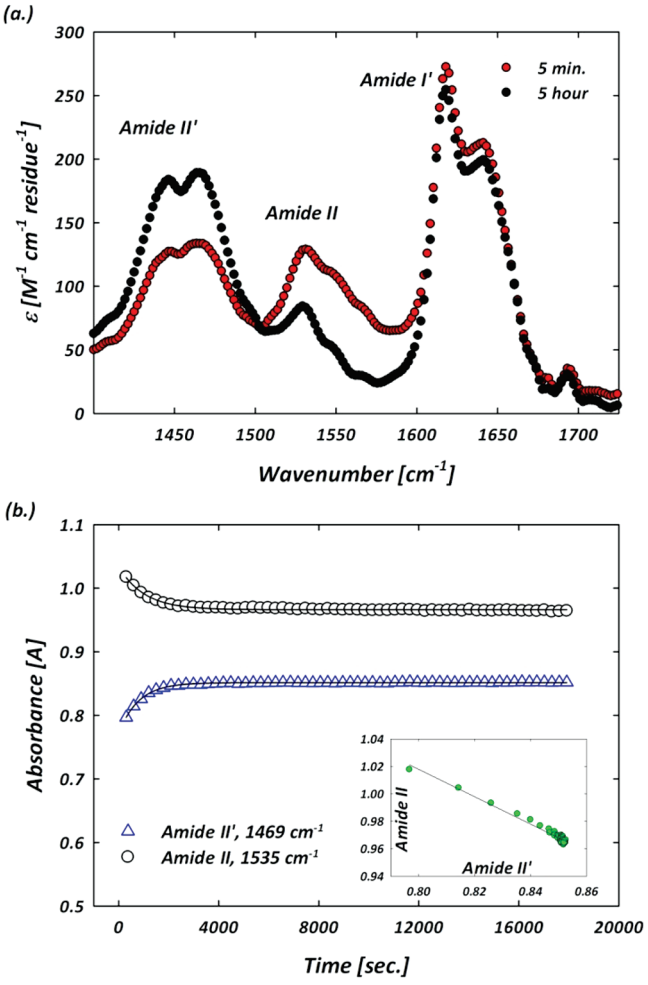

Figure 5. (a) FTIR spectra of a 10 mg/mL AK-16 solution measured at both 5 min (red) and 5 h (black) after dissolving the peptide in D_2O. (b) Kinetics of the amide II′ (blue triangles) and amide II (black circles) bands probed at 1469 and 1535 cm^{-1}, respectively, both of which can be fit with a single-exponential function using the time constant reported for the fast phase of the UV-CD kinetic analysis, namely 18 min. Inset: a plot of amide II vs amide II′ peak intensities. The negative linear correlation reflects H-D exchange of backbone amide protons.

peptide concentrations of 5 mg/mL. It is clear that each of these peptides adopts a mixture of α-helical and PPII conformations, depending on whether the side chains are uncharged or charged, respectively.[27] This observation is consistent with homopolypeptides of amino acids containing ionizable side chains.[28] AFM images show no indication of AO-16, AE-16, or AK-12 aggregation (not shown). In contrast to these results, AR-16 behaves in a way similar to that of AK-16 in solution. In particular, AR-16 forms soluble, thermodynamically unstable β-sheet-rich aggregates upon dissolution in deuterated water. AFM images of AR-16 depict a filamentous network similar to that which is observed for AK-16 (Figure 1d).

AK-16 Hydrogel Formation as a Function of Salt and Secondary Structure. Upon salt addition, AK-16 solutions instantaneously form macroscopic hydrogels at concentrations >~5 mg/mL (Figure 7a). This is consistent with hydrogel formation observed for other self-assembling oligopeptides.[2] The AK-16 hydrogel shows a nanoweb-like architecture, as seen in the AFM image shown in Figure 1b. To study the salt dependence of the physicochemical properties of the AK-16 hydrogels, we measured the UV-CD spectra of AK-16 in the presence of various salts, including

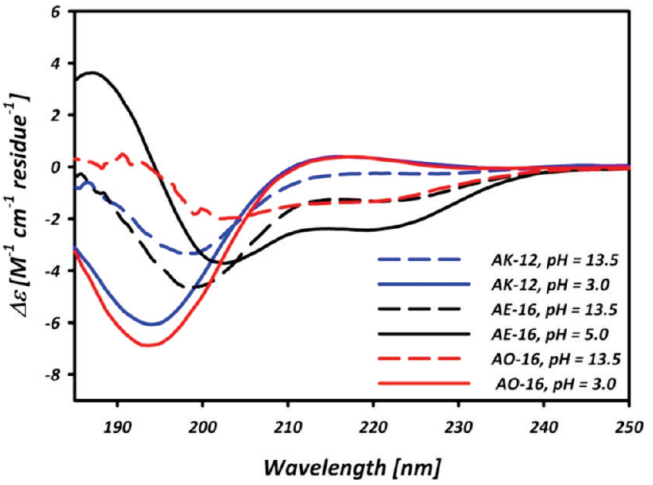

Figure 6. UV-CD spectra of AO-16 (dash-dash), AE-16 (solid), and AK-12 (dash-dot-dash), measured at 25 °C, at two indicated pH values. The negative maxima at 208 and 222 nm reflect α-helical conformations, while the positive and negative maxima at 220 and 198 nm, respectively, are indicative of PPII-like conformations.

NaCl, CsCl, $MgCl_2$, and Na_3PO_4. As shown in Figure S2a, salt addition stabilizes the underlying β-sheet secondary structure, resulting in a narrowing of the negative maximum at 215 nm in the UV-CD spectrum. The valency of salt ions can have a large effect on the types of aggregates formed by oligopeptides.[15] We found that the position of the negative maximum in the UV-CD spectra is blue-shifted when multivalent salts are added, relative to the position in the presence of monovalent salts. Similar results have recently been observed for EMK16-II, where the blue shift of the negative UV-CD band is attributed to the formation of more compact and amorphous aggregates observed in the presence of multivalent ions.[15] The FTIR spectra of AK-16 as a function of the various salts (Figure S2b) show a downshift of the amide I′ band from 1618 cm^{-1} in the absence of salt to 1616 cm^{-1} in the presence of the monovalent salts NaCl and CsCl, at concentrations of 1 M, to 1614 cm^{-1} in the presence of the multivalent salts, $MgCl_2$ and Na_3PO_4. The amide I′ downshift results from stronger coupling of the backbone carbonyl stretching vibrations[29] and is consistent with the formation of more compact β-sheet-rich aggregates.[15]

To elucidate the rheological properties of AK-16 hydogels, we measured the viscosity as a function of shear rate for AK-16 hydrogels prepared with varying NaCl concentrations. At peptide concentrations of 5 and 10 mg/mL and NaCl concentrations ranging from 1 to 2 M, shear-thinning behavior is observed, in which the viscosity of the hydrogel decreases as a function of shear rate, as shown in Figure 7b. Such behavior is a defining characteristic of oligopeptide hydrogels.[16] Higher salt and peptide concentrations yield more viscous hydrogels. Owing to the prerequisite of β-sheet structures to yield stable hydrogels, we attempted to exploit the conformational instability of the AK-16 β-sheets to essentially tune the viscosity of the resulting hydrogel. We prepared two separate AK-16 hydrogels from the same 5 mg/mL peptide stock solution, one of which was prepared with the fresh stock solution and the other from a portion of the solution which was allowed to incubate overnight at room temperature. As shown in Figure 7b, the hydrogel prepared from the incubated solution exhibited a much lower viscosity than that which was prepared with a fresh sample, yet still resulted in shear-thinning behavior.

Slow Release of a Model Protein from AK-16 Hydrogels. Owing to the inherent biocompatibility and wide range of

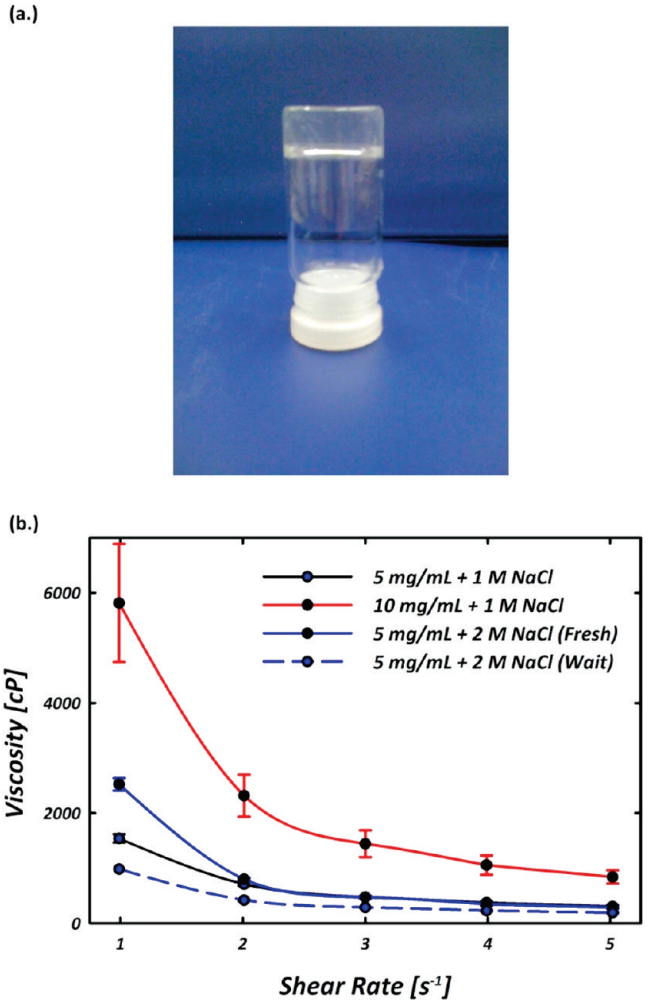

Figure 7. (a) Self-supporting AK-16 hydrogel (5 mg/mL AK-16 w/2 M NaCl). (b) Viscosity of AK-16 hydrogels as a function of shear rate. Hydrogels were prepared with 5 mg/mL AK-16 and 1 M NaCl (black) and 10 mg/mL AK-16 and 1 M NaCl (red). To illustrate how β-sheet structure effects the viscosity of the resulting hydrogel, NaCl was added both to a freshly prepared portion of a 5 mg/mL AK-16 solution (blue, solid) and to a portion which was allowed to incubate overnight at room temperature (blue, dash) to yield as resulting salt concentration of 2 M. All samples were measured a total of three times. The decrease in viscosity vs shear rate is indicative of shear-thinning behavior and characteristic of peptide-based hydrogels.

pH values at which the system should be operable (i.e., below the pK_a of the Lys side chain), we illustrated the application of AK-16 hydrogels as potential drug delivery systems by incorporating a model protein, namely cytochrome *c*, into the AK-16 matrix, and monitored the release of the protein from the hydrogel via UV absorption spectroscopy. The release profiles are shown in Figure 8 for different AK-16 and protein concentrations. The diffusion coefficient of cytochrome *c* was determined as described in ref 9 and found to be nearly independent of the protein concentration and slightly dependent on the concentration of AK-16 in the hydrogel. In particular, we obtained a diffusion coefficient of $(0.61 \pm 0.05) \times 10^{-10}$ m^2/s for cytochrome *c* released from the 10 mg/mL AK-16 hydrogel and $(0.52 \pm 0.05) \times 10^{-10}$ m^2/s for cytochrome *c* released from the 5 mg/mL AK-16 hydrogel. The magnitude of these values is consistent with those of proteins of similar size released from RADA-16 hydrogels.[9] The similarity of the UV-CD spectrum of cytochrome *c* released from the AK-16 hydrogel with that in aqueous solution (Figure S3) suggests that AK-16 hydrogels can be

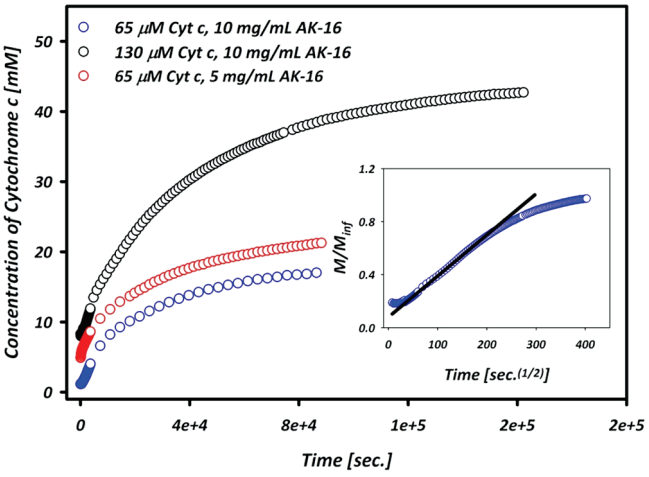

Figure 8. Slow release experiments of cytochrome *c* (cyt *c*) encapsulated in AK-16 hydrogels (prepared with 1 M NaCl) with the following peptide and protein concentrations: 10 mg/mL AK-16 + 65 μM cyt *c* (blue), 10 mg/mL AK-16 + 130 μM cyt *c* (black), and 5 mg/mL AK-16 + 65 μM cyt *c* (red). Cytochrome *c* release was monitored via the absorption at 275 nm. Inset: plot of $[\text{cyt } c]_t/[\text{cyt } c]_\infty$ vs $(\text{time})^{1/2}$. The slope of the linear portion is used to calculate the protein diffusion coefficient as described in the Materials and Methods section.

used to encapsulate and release model proteins while maintaining their native secondary structure. It should be noted that the values of the diffusivities obtained from hydrogels of different AK-16 concentrations are within the uncertainty of each other. This is expected owing to the small hydrodynamic radius of cytochrome *c* compared with the pore sizes of the hydrogel matrix, which are 2−3 orders of magnitude larger.

Discussion

The ability of AK-16 to adopt β-sheet secondary structures comes as a surprise since alanine-rich peptides of similar length and amino acid composition typically adopt α-helical conformations in aqueous solutions.[30,31] The sequence positions of the positively charged lysine residues should prevent the formation of such sheet structures via electrostatic repulsion. In contrast to expectations, the time-dependent UV-CD and FTIR spectroscopic measurements indicate a predominance of thermodynamically unstable β-sheet structures which spontaneously decay into more flexible, PPII-like conformations. Biphasic kinetics are observed for the conformational decay, as probed by the UV-CD spectra, where the fast phase reflects the slow hydration of AK-16 aggregates, as confirmed by the H−D exchange process observed by the temporally resolved FTIR spectra. These results suggest that preformed β-sheet aggregates in the solid state, which would be expected to dissociate upon dissolution in water, are somewhat stabilized and exhibit slow hydration kinetics. Indeed, the attenuated total reflectance (ATR) spectrum of AK-16 powder confirms the predominance of an antiparallel β-sheet conformation in the solid state (Figure S4).[23] This behavior is different from what is generally reported in the literature about more conventional self-aggregating peptides, which dissolve quickly into monomers in aqueous solution and recombine into aggregates only after a nucleation process has taken place[32] and those which assemble under well-defined and controlled conditions.[2]

The percentage of PPII-like conformations present after 300 min (relative to the initial 5 min spectra) can be gauged by the intensity of the positive maximum at 220 nm. As shown in the inset of Figure 3, the PPII percentage exhibits a negative linear correlation with the AK-16 concentration. The decay of the AK-16 β-sheet conformation into PPII-like conformations suggests a link between these two conformations. This finding offers support for the hypothesis put forward by Blanch et al. suggesting that PPII may be the "killer" conformation in the various "conformational" diseases, since PPII conformations appear to precede the β-sheet conformational switch, which is concurrent with fibril formation.[33]

The ability of AR-16 to self-assemble into well-ordered structures similar to those of AK-16, together with the fact that neither AO-16 nor AE-16 aggregates under similar conditions, suggests that the lengths of the side chains are defining features of $(AAxA)_4$ β-sheet aggregates. The side chains of both Lys and Arg are of similar lengths, while Orn and Glu are slightly shorter. Owing to the similar functionality of the Lys and Orn side chains, this finding provides strong evidence that intermolecular and possibly intramolecular hydrogen bonds are initially formed between the Lys side chains and the peptide backbone, which can stabilize β-sheet structures. Without the addition of stabilizing elements, e.g. salt, electrostatic repulsion of the Lys/Arg side chains results in the spontaneous decay of the β-sheet structures, with the concurrent hydration of the backbone, until a slow-approaching equilibrium is reached among the different conformations. β-sheet stabilization and thus hydrogel formation result from the shielding of the lysine side chain charges, which can then allow for such an extended structure, with the lysine side chains all residing on the same face of the sheet.

Sequence length is important for self-assembly and β-sheet formation. This is evidenced by the fact that AK-12 does not aggregate under conditions similar to those promoting AK-16 self-assembly, even at concentrations 5 times larger than those used for AK-16 and AR-16 (not shown). It is plausible that only the two central AAKA segments of AK-16 are involved in the β-sheet formation, so that end effects dominating in the case of AK-12 prevent such behavior. In fact, the aggregation and β-sheet formation of many disease-related peptides and proteins are thought to be initiated by short motifs, or "self-recognition elements" (SRE's), which contain only a few amino acid residues.[34,35]

β-sheet structure is a prerequisite for hydrogel formation by AK-16. Stabilization of AK-16 β-sheet aggregates can be achieved via the addition of various salts to yield a self-supporting hydrogel with an underlying nanoweb-like architecture. The viscosity and physicochemical properties of the hydrogel depend on the type of salt used, the salt and peptide concentrations, and the amount of β-sheet secondary structure present. The underlying fibrillar network of AK-16 hydrogels allows for the encapsulation and slow release of a model protein, illustrating the potential of such a system for drug delivery. Since β-sheet structure is a prerequisite for AK-16 hydrogel formation, the initial conformational instability of such structures presents AK-16 as a unique class of hydrogel-forming oligopeptides, where the conformational instability can be exploited as a means to tune the viscosity and physicochemical properties of the resultant hydrogel.

In summary, we have characterized the spontaneous and unexpected self-assembly of the alanine-rich oligopeptide AK-16. AK-16 disobeys typical sequence requirements for peptide self-assembly, yet forms thermodynamically unstable β-sheet structures, which decay with time. The aggregation propensity of AK-16 is attributed to the length of the lysine side chain, which can allow for the formation of intermolecular and possibly intramolecular hydrogen bonding to the peptide backbone upon dissolution. Stabilization of the unstable AK-16 β-sheet structures via salt addition results in the formation of a hydrogel for potential biotechnological and biomedical applications. The viscosity and physicochemical properties of the resulting hydrogel can be tuned by factors such as salt type and concentration, peptide concentration, and β-sheet content. Taken together, these results illustrate the unique conformational properties of a novel

class of self-assembling oligopeptides and offer insight into *de novo* design of self-assembling peptides for the creation of novel biomaterials.

Materials and Methods

Ac-$(AAKA)_4$-NH_2 (AK-16, >98% purity), Ac-$(AAEA)_4$-NH_2 (AE-16, >98% purity), Ac-$(AARA)_4$-NH_2 (AR-16, >98% purity), Ac-$(AAOA)_4$-NH_2 (AO-16, >98% purity), and Ac-$(AAKA)_3$-NH_2 were synthesized by Celtek Peptides (Nashville, TN) and used without further purification. D_2O, CsCl, Na_3PO_4, and $MgCl_2$ were purchased from Sigma-Aldrich. NaCl was purchased from Acros Organics. Equine cytochrome *c* was purchased from Sigma-Aldrich and used without further purification. Peptide solutions for the UV-CD and FTIR spectroscopic time-dependent measurements were prepared as follows. A preweighed amount of solid peptide was dissolved in D_2O, and the sample was vortexed for ~1 min. This resulted in nonturbid, homogeneous samples.

UV-CD. All UV-CD spectra were measured using a Jasco J-810 spectropolarimenter, using a data pitch of 0.05 nm, a response time of 1 s, a bandwidth of 5 nm, a scan speed of 500 nm/min, and a wavelength window of 180−300 nm. The instrument was purged with N_2 during the course of the measurements. For all UV-CD measurements, peptide stock solutions were diluted 10-fold with D_2O and were placed in a 50 μm Q Silica UV-Grade demountable cell (International Crystal Laboratories). Temperature was controlled inside the chamber using a Peltier temperature controller (Jasco). The representative time-dependent UV-CD spectra shown in Figure 2 were measured beginning 300 s (5 min) after sample preparation, while the kinetic data shown in Figure 4 were obtained from measurements which were started ~120 s (2 min) after sample preparation. This was necessary to obtain a satisfactory fit of the fast phase of the kinetic data. Measurements of AK-16 with various salts were prepared by the addition of a freshly prepared solution of 5 mg/mL AK-16 to a preweighed amount of salt.

Controlled Release. Cytochrome *c* encapsulated AK-16 hydrogels were prepared as follows. A preweighed amount of AK-16 was dissolved in a solution of cytochrome *c* in D_2O solution with a protein concentration of either 1 or 2 mg/mL. This solution was transferred to a 10 mm quartz cell (Helma), and a saturated NaCl solution (in D_2O) was added dropwise to yield a final AK-16 of either 5 or 10 mg/mL and a final NaCl concentration of 1.0 M. Because of dilution with the saturated NaCl solution, this procedure yielded an encapsulated cytochrome *c* concentration of either 65 or 130 μM, depending on the initial protein stock solution used. 500 μL of D_2O was carefully placed on top of the AK-16 hydrogel containing cytochrome *c*, and the system was placed into the nitrogen-purged sample chamber of a Jasco J-810 spectropolarimeter. Cytochrome *c* diffusion into the upper water layer was monitored via absorbance at 275 nm, resulting from the aromatic residues in the protein. A control experiment, containing no cytochrome *c*, was performed to establish a baseline for the release profiles.

The diffusion coefficient of cytochrome *c* was determined via the method reported in ref 9, using a variation of Fick's second law of diffusion, given as

$$\frac{[\text{cyt } c]_t}{[\text{cyt } c]_\infty} = \left(\frac{16 D_{\text{app}} t}{\pi H^2}\right)^{1/2}$$

where D_{app} is the apparent diffusion coefficient, t is time, and $[\text{cyt } c]_t$ and $[\text{cyt } c]_\infty$ are the concentration of cytochrome *c* released at time, t, and infinite time, respectively. H is the height of the hydrogel, which was determined using the dimensions of the employed cuvette and the volume of the hydrogel. D_{app} was obtained from the slope of the linear portion of a plot of $[\text{cyt } c]_t/[\text{cyt } c]_\infty$ vs $t^{1/2}$.

FTIR. FTIR spectra were measured with a ChiralIR spectrometer from BioTools (Jupiter, FL). The peptide solutions were placed in a 100 μm CaF_2 BioCell (BioTools). Spectra were collected at 5 min intervals over a course of 5 h, using 8 cm^{-1} resolution, and were solvent corrected. Three scans were averaged at each time interval. The instrument was purged with N_2 during the course of the measurements.

Atomic Force Microscopy (AFM). All AFM experiments were performed at room temperature, using a multimode atomic force microscope (Nanoscope IIIa; Digital Instruments, Santa Barbara, CA), equipped with an E-type piezoscanner. AK-16 samples were prepared as described above. 15 μL of the AK-16 solution/hydrogel sample was deposited onto a freshly cleaved mica surface and allowed to sit for ~15 s, after which a steady stream of N_2 gas was employed to dry the sample. Tapping-mode imaging was carried out with a silicon probe (TESP) from Veeco (Camarillo, CA). Height and deflection images of the gelled and nongelled samples were obtained with a scan rate of 1 Hz.

Rheological Measurements. AK-16 hydrogel samples for rheological measurements were prepared by adding a freshly prepared AK-16 in D_2O solution to a preweighed amount of salt. Additionally, a sample of 5 mg/mL AK-16 was left to incubate overnight at room temperature prior to hydrogelation to investigate the effect of conformational relaxation and, in particular, β-sheet decay on the hydrogel viscosity. Viscosity of the peptide hydrogel samples was measured using a Brookfield DV-III Ultra viscometer/rheometer using a Wells-Brookfield CPE-42 cone spindle. The absolute viscosity of ~1 mL of the peptide hydrogel was obtained via a "cone−plate"-like method, with a cone angle of 1.5° and a spindle radius of 2.4 cm. Data were obtained using the Rheocalc software (Brookfield Engineering Laboratories) and automatically acquired over RS232. After zeroing the instrument, ~1 mL of the peptide hydrogel sample was allowed to equilibrate on the plate at room temperature for 15−20 min. The shear rate was then varied from 1 to 5 s^{-1} and then back to 1 s^{-1}, at intervals of 1 s^{-1}. The shear stress [dyne/cm^2] was measured after 3 min at each speed to ensure that data were collected at equilibrium. A total of three trials were performed for each sample, and the results were averaged.

Acknowledgment. This work was supported by an NSF grant (Chem 0804492) to R.S.S.

Supporting Information Available: Additional CD and IR spectra. This material is available free of charge via the Internet at http://pubs.acs.org.

References and Notes

(1) Whitesides, G. M.; Mathias, J. P.; Seto, C. T. *Science* **1991**, *254*, 1312–1319.
(2) Zhang, S.; Altman, M. *React. Funct. Polym.* **1999**, *41*, 91–102.
(3) Dobson, C. M. *Nat. Rev. Drug Discovery* **2003**, *2*, 154–160.
(4) Chiti, F.; Dobson, C. M. *Annu. Rev. Biochem.* **2006**, *75*, 333–366.
(5) Lee, H.-g.; Zhu, X.; Petersen, R. B.; Perry, G.; Smith, M. A. *Curr. Med. Chem. Immunol. Endocr. Metab. Agents* **2003**, *3*, 293–298.
(6) Nelson, R.; Sawaya, M. R.; Balbirnie, M.; Madsen, A. Ø.; Riekel, C.; Grothe, R.; Eisenberg, D. *Nature* **2005**, *435*, 773–778.
(7) Serpell, L. C.; Fraser, P. E.; Sunde, M. *Method. Enzymol.* **1999**, *309*, 526–536.
(8) Connelly, S.; Choi, S.; Johnson, S. M.; Kelly, J. W.; Wilson, I. A. *Curr. Opin. Struct. Biol.* **2010**, *20*, 54–62.
(9) Koutsopoulos, S.; Unsworth, L. D.; Nagai, Y.; Zhang, S. *Proc. Natl. Acad. Sci. U.S.A.* **2009**, *106*, 4623–4628.
(10) Nagai, Y.; Unsworth, L. D.; Koutsopoulos, S.; Zhang, S. *J. Controlled Release* **2006**, *115*, 18–25.
(11) Holmes, T. C.; Lacalle, S. D.; Su, X.; Liu, G.; Rich, A.; Zhang, S. *Proc. Natl. Acad. Sci. U.S.A.* **2000**, *97*, 6728–6733.
(12) Zhang, S.; Holmes, T. C.; DiPersio, C. M.; Hynes, R. O.; Su, X.; Rich, A. *Biomaterials* **1995**, *16*, 1385–1393.
(13) Ruan, L.; Zhang, H.; Luo, H.; Liu, J.; Tang, F.; Shi, Y.-K.; Zhao, X. *Proc. Natl. Acad. Sci. U.S.A.* **2009**, *106*, 5105–5110.
(14) Kisiday, J.; Jin, M.; Kurz, B.; Hung, H.; Semino, C.; Zhang, S.; Grodzinsky, A. J. *Proc. Natl. Acad. Sci. U.S.A.* **2002**, *99*, 9996–10001.

(15) Zou, D.; Tie, Z.; Lu, C.; Qin, M.; Lu, X.; Wang, M.; Wang, W.; Chen, P. *Biopolymers* **2010**, *93*, 318–329.
(16) Schneider, J. P.; Pochan, D. J.; Ozbas, B.; Rajagopal, K.; Pakstis, L.; Kretsinger, J. *J. Am. Chem. Soc.* **2002**, *124*, 15030–15037.
(17) Measey, T. J.; Schweitzer-Stenner, R. *J. Am. Chem. Soc.* **2006**, *128*, 13324–13325.
(18) Klunk, W. E.; Jacob, R. F.; Mason, R. P. *Methods Enzymol.* **1999**, *309*, 285–305.
(19) Sreerama, N.; Woody, R. W. *Methods Enzymol.* **2004**, *383*, 318–351.
(20) Schweitzer-Stenner, R.; Measey, T. J. *Proc. Natl. Acad. Sci. U.S.A.* **2007**, *104*, 6649–6654.
(21) Woody, R. W. *J. Am. Chem. Soc.* **2009**, *131*, 8234–8245.
(22) Krimm, S.; Bandekar, K. *Adv. Protein Chem.* **1986**, *38*, 181–364.
(23) Barth, A. *Biochim. Biophys. Acta* **2007**, *1767*, 1073–1101.
(24) Jang, S.; Yuan, J.-M.; Shin, J.; Measey, T. J.; Schweitzer-Stenner, R.; Li, F.-Y. *J. Phys. Chem. B* **2009**, *113*, 6054–6061.
(25) Schweitzer-Stenner, R. *Vib. Spectrosc.* **2006**, *42*, 98–117.
(26) Woodward, C. *Trends Biochem. Sci.* **1993**, *18*, 359–360.
(27) Woody, R. W. Theory of Circular Dichroism of Proteins. In *Circular Dichroism and the Conformational Analysis of Biomolecules*; Fasman, G. D., Ed.; Plenum Press: New York, 1996; pp 25−67.
(28) Tiffany, M. L.; Krimm, S. *Biopolymers* **1968**, *6*, 1379–1382.
(29) Lee, C.; Cho, M. *J. Phys. Chem. B* **2004**, *108*, 20397–20407.
(30) Marqusee, S.; Robbins, V. H.; Baldwin, R. L. *Proc. Natl. Acad. Sci. U.S.A.* **1989**, *86* (14), 5286–5290.
(31) Chakrabartty, A.; Kortemme, T.; Baldwin, R. L. *Protein Sci.* **1994**, *3*, 843–852.
(32) Auer, S.; Dobson, C. M.; Vendruscolo, M.; Maritan, A. *Phys. Rev. Lett.* **2008**, *101*, 258101.
(33) Blanch, E. W.; Morozova-Roche, L. A.; Cochran, D. A. E.; Doig, A. J.; Hecht, L.; Barron, L. D. *J. Mol. Biol.* **2000**, *301*, 553–563.
(34) Sawaya, M. R.; Sambashivan, S.; Nelson, R.; Ivanova, M. I.; Sievers, S. A.; Apostol, M. I.; Thompson, M. J.; Balbirnie, M.; Wiltzius, J. J. W.; McFarlane, H. T.; Madsen, A. Ø.; Riefel, C.; Eisenberg, D. *Nature* **2007**, *447*, 453–457.
(35) Tzotzos, S.; Doig, A. J. *Protein Sci.* **2010**, *19*, 327–348.